J|A|C|S
ARTICLES
Published on Web 11/25/2003

Pseudomultidimensional NMR by Spin-State Selective Off-Resonance Decoupling

Christy Rani R. Grace and Roland Riek*

Contribution from the Structural Biology Laboratory, The Salk Institute, La Jolla, California 92037

Received April 17, 2003; E-mail: riek@sbl.salk.edu

Abstract: An alternate technique for accurately monitoring the chemical shift in multidimensional NMR experiments using spin-state selective off-resonance decoupling is presented here. By applying off-resonance decoupling on spin *S* during acquisition of spin *I*, we scaled the scalar coupling $J(I,S)$ between the spins, and the residual scalar coupling turns out to be a function of the chemical shift of spin *S*. Thus, the chemical shift information of spin *S* is indirectly retained, without an additional evolution period and the accompanying polarization transfer elements. The detection of the components of the doublet using spin-state selection enables an accurate measurement of the residual scalar coupling and a precise value for the chemical shift, concomitantly. The spin-state selection further yields two subspectra comprising either one of the two components of the doublet and thereby avoiding the overlap problems that arise from off-resonance decoupling. In general, spin-state selective off-resonance decoupling can be incorporated into any pulse sequence. Here, the concept of spin-state selective off-resonance decoupling is applied to 3D ^{13}C or ^{15}N-resolved [^{1}H,^{1}H]-NOESY experiments, adding the chemical shift of the heavy atom attached to the hydrogen (^{13}C or ^{15}N nuclei) with high resolution resulting in a pseudo-4D. These pseudo-4D heavy-atom resolved [^{1}H, ^{1}H]-NOESY experiments contain chemical shift information comparable to that of 4D ^{13}C or ^{15}N-resolved [^{1}H,^{1}H]-NOESY, but with an increase in chemical shift resolution by 1−2 orders of magnitude.

Introduction

Three-dimensional heteronuclear NMR experiments offer dramatic improvements in spectral resolution by spreading through-bond and through-space correlations along the three orthogonal frequency axes. These experiments have resulted in a major breakthrough in structural biology (i) by increasing the limit on the molecular size of the proteins for three-dimensional structure determination and structure−activity relationship[2] and (ii) by reducing the time required for the structure determination using automated procedures.[3,4] It is evident that an extension of these experiments to four dimensions would further improve the spectral resolution and concomitantly result in a large collection of unambiguous through-bond and through-space correlations. Therefore, such an improvement might open an avenue for automated high-throughput structure determination[5] and also increase the limit on the molecular size of the proteins for three-dimensional structure determination.

However, the extension to four dimensions (4D) has its limitations, because the additional dimension results in (i) low spectral resolution due to limited measuring time[6] and (ii) extensive signal loss during the additional polarization transfer elements and evolution periods due to relaxation. These limitations are the inherent properties of time-domain spectroscopy,[7] in which one chemical shift dimension is observed directly, whereas in the so-called indirect dimensions (in 4D there are three indirect dimensions), the chemical shift evolution is monitored indirectly during the evolution times.[6] For example, a 4D ^{13}C-resolved [^{1}H,^{1}H]-NOESY[8] experiment contains two polarization transfer periods and one additional evolution time more than the corresponding 3D version, which results in major signal loss. For a small protein with a rotational correlation time τ_c of 4 ns, the signal loss is approximately a factor of 3 (data not shown). Also, the improvement in resolution is only marginal due to the limited overall measuring time. For example, a typical 3D ^{13}C-resolved [^{1}H,^{1}H]-NOESY experiment with a digital resolution of 25 Hz [^{1}H] × 60 Hz [^{13}C] × 4 Hz [^{1}H] (150($t1$[^{1}H]) × 50($t2$[^{13}C]) × 1024($t3$[^{1}H acquisition]) complex points) and a phase cycle of 4 requires about 40 h of measuring time. The corresponding 4D ^{13}C-resolved [^{1}H,^{1}H]-NOESY with only a digital resolution of 25 Hz [^{1}H] × 170 Hz [^{13}C] × 170

(1) Abbreviations: CRINEPT, cross-correlated relaxation-enhanced polarization transfer; FID, free induction decay; NMR, nuclear magnetic resonance; NOE, nuclear Overhauser enhancement; PFG, pulsed field gradient; 2D, 3D, 4D, two-dimensional, three-dimensional, four-dimensional; SITAR, spin-state selective off-resonance decoupling; S3E, spin-state selection element; TROSY, transverse relaxation optimized spectroscopy.

(2) Riek, R.; Fiaux, J.; Bertlesen, E. B.; Horwich, A. L.; Wüthrich, K. *J. Am. Chem. Soc.* **2002**, *124*, 12144−12153.
(3) Güntert, P. *Q. Rev. Biophys.* **1998**, *31*, 145−237.
(4) Linge, J. P.; O'Donoghue, S. I.; Nilges, M. *Methods Enzymol*. **2001**, *339*, 71−90.
(5) Grishaev, A.; Llinas, M. *Proc. Natl. Acad. Sci. U.S.A.* **2002**, *99*, 6707−6712.
(6) Wider, G. *Prog. Nucl. Magn. Reson. Spectrosc*. **1998**, *32*, 193−275.
(7) Ernst, R. R.; Bodenhausen, G.; Wokaun A. *Principles of Nuclear Magnetic Resonance in One and Two Dimensions*; Clarendon Press: Oxford, 1985.
(8) Kay, L. E.; Clore, G. M.; Bax, A.; Gronenborn, A. M. *Science* **1990**, *249*, 411−414.

10.1021/ja035689x CCC: $25.00 **© 2003 American Chemical Society**

Hz [^{13}C] × 4 Hz [^{1}H] (150(*t*1[^{1}H]) × 10(*t*2[^{13}C]) × 10(*t*3[^{13}C]) × 1024(*t*4[^{1}H acquisition]) complex points) requires a measuring time of 7 days. Nevertheless, it is only the use of 4D versions of the ^{15}N-resolved [^{1}H,^{1}H]-NOESY[8] and 4D TROSY-HNCA-CO and HNCOCA experiments applied to deuterated proteins[9] that has enabled the backbone assignment of a ~700 residue protein.[10,11]

To overcome the inherent problem of low chemical shift resolution in 4D experiments, the concept of "reduced dimensionality" was introduced.[12] Here, the information during two different evolution periods is obtained by incrementing both of the evolution times together as in one dimension. The projection of two dimensions into one dimension reduces the measuring time of the experiment and hence yields high resolution. However, reduced dimensionality experiments suffer from extensive signal loss due to additional polarization transfer pulses and evolution periods,[13] because the concept of reduced dimensionality is also based on time-domain spectroscopy.[7] Recently, our group has introduced an alternative concept for chemical shift monitoring. The concept of chemical shift coding increases the number of correlations (dimensions) by one without additional polarization transfer pulses and evolution periods and hence overcomes the inherent problems of time-resolved spectroscopy mentioned above.[14] The chemical shift monitored is coded in the line-shape of the cross-peak through an apparent residual scalar coupling active during the evolution or acquisition period. The size of the scalar coupling is manipulated with a Gaussian radio frequency pulse. This technique has been successfully demonstrated by applying it to small ^{13}C,^{15}N-labeled proteins and large ^{2}H,^{13}C,^{15}N-labeled proteins in triple resonance experiments.[15,16]

Here, another alternate technique for monitoring chemical shift accurately is presented, which extensively supersedes the other techniques discussed above. The proposed technique combines the use of off-resonance decoupling along with the pulse sequence for spin-state selection. Off-resonance decoupling has been used extensively in premultidimensional NMR history[17,18] and for one specific problem in a multidimensional experiment.[19] Off-resonance decoupling on spin *S* during acquisition of spin *I* results in chemical shift-dependent residual scalar coupling between the spins. The residual scalar coupling is a function of the chemical shift of the heteronucleus, and hence off-resonance decoupling increases the number of detected frequencies by one without the use of additional polarization transfer elements and evolution periods. Similar to the heteronuclear E. COSY experiment,[20] spin-state selection detects the two components of the doublet from off-resonance decoupling independently, which results in the accurate measurement of the residual scalar couplings and also of the chemical shifts, concomitantly. Here, the concept of spin-state selective off-resonance decoupling (SITAR) is applied to two NOESY experiments, (i) the 3D ^{15}N-resolved [^{1}H,^{1}H]-NOESY experiment, where the chemical shifts of ^{15}N are monitored indirectly during acquisition, resulting in a pseudo-4D experiment. The pseudo-4D ^{15}N-resolved [^{15}N−^{1}H,^{1}H−^{15}N]-NOESY contains the chemical shifts of the two involved hydrogens and the chemical shifts of their attached ^{15}N per NOE, in contrast to the conventional 3D ^{15}N-resolved [^{1}H,^{1}H]-NOESY experiment, where only one ^{15}N chemical shift is known per NOE. (ii) SITAR is also applied to the 3D ^{13}C-resolved [^{1}H,^{1}H]-NOESY experiment, resulting in the pseudo-4D ^{13}C-resolved [^{13}C−^{1}H,^{1}H−^{13}C/^{15}N]-NOESY. The additional SITAR-monitored chemical shifts enhance the resolution of the spectra by 2 orders of magnitude, when compared with the conventional 3D ^{13}C-resolved or ^{15}N-resolved [^{1}H,^{1}H]-NOESY experiments.

Theory

Consider a system of two scalar coupled spins, *I* and *S* of spin $^{1}/_{2}$, with a scalar coupling constant $^{1}J(I,S)$ located in the molecule. During the acquisition time *t* (or evolution time *t*), spin-*I* evolves under its chemical shift and the scalar coupling $^{1}J(I,S)$, giving rise to a doublet in the Fourier transformed spectrum. They can be described using single transition basis operator I^{-}_{24} and I^{-}_{13}, denoting transitions $2 \rightarrow 4$ and $1 \rightarrow 3$ in the standard energy-level diagram for a system of two spins $^{1}/_{2}$, and are associated with the frequencies $\omega(I_{24})$ and $\omega(I_{13})$ (Figure 1A) given by

$$I^{-}_{24} = I_x + 2I_xS_z \qquad \omega(I_{24}) = \omega(I) - \pi^{1}J(I,S) \quad (1)$$

$$I^{-}_{13} = I_x - 2I_xS_z \qquad \omega(I_{13}) = \omega(I) + \pi^{1}J(I,S) \quad (2)$$

If continuous wave off-resonance decoupling is applied during time *t* on spin *S*, at a frequency ω_{cw} of radio frequency power $\gamma_S B_2/2\pi$, the scalar coupling $^{1}J(I,S)$ has been shown to be a function of the chemical shift of spin *S*.[17,18,21] If $\omega_{cw} - \omega_S$ is large as compared with $0.5\,^{1}J(I,S)$ and the decoupling time *t* is long, the observed residual coupling is given by[21]

$$^{R}J(I,S) \approx \{(\omega_{cw} - \omega_S)/[(\omega_{cw} - \omega_S)^2 + (\gamma_S B_2/2\pi)^2]^{0.5}\}\,^{1}J(I,S) \quad (3)$$

with the frequencies of the doublet (Figure 1B) given by

$$\omega(I_{24}) = \omega(I) - \pi^{R}J(I,S) \quad (4)$$

$$\omega(I_{13}) = \omega(I) + \pi^{R}J(I,S) \quad (5)$$

Equation 3 can be rewritten as

$$\omega_S = \omega_{cw} \pm [^{R}J(I,S)(\gamma_S B_2/2\pi)/[^{1}J(I,S)^2 - {}^{R}J(I,S)^2]^{0.5}] \quad (6)$$

From eqs 3−6 it is evident that the chemical shift of spin *S*, ω_S, can be monitored from the residual scalar coupling. Furthermore, it is evident that the accuracy of the determination of the chemical shift of spin *S* depends directly on the scalar

(9) Yang, D.; Kay, L. E. *J. Am. Chem. Soc.* **1999**, *121*, 2571−2575.
(10) Tugarinov, V.; Muhandiram, R.; Ayed, R.; Kay, L. E. *J. Am. Chem. Soc.* **2002**, *124*, 10025−10035.
(11) Yang, D., personal communication.
(12) Szyperski, T.; Wider, G.; Bushweller, J.; Wüthrich, K. *J. Am. Chem. Soc.* **1993**, *115*, 9307−9308.
(13) Sattler, M.; Schleucher, J.; Griesinger, C. *Prog. Nucl. Magn. Reson. Spectrosc.* **1999**, *34*, 93−158.
(14) Kwiatkowski, W.; Riek, R. *J. Biomol. NMR.* **2003**, *25*, 281−290.
(15) Ritter, C.; Luhrs, T.; Kwiatkwoski, W.; Riek, R. *J. Biomol. NMR*, in press.
(16) Pegan, S.; Kwiatkwoski, W.; Senyon, C.; Riek, R. *J. Magn. Reson.*, in press.
(17) Ernst, R. R. *J. Chem. Phys.* **1966**, *45*, 3845−3850.
(18) Tanabe, M.; Hamasaki, T.; Thomas, T. *J. Am. Chem. Soc.* **1971**, *93*, 273−274.
(19) Fesik, S. W.; Eaton, H. L.; Olejniczak, E. T.; Gampe, R. T. *J. Am. Chem. Soc.* **1990**, *112*, 5370−5371.
(20) Meissner, A.; Duus, J. *ϕ.*; Sørensen, O. W. *J. Magn. Reson.* **1997**, *128*, 92−97.
(21) Freeman, R. *A Handbook of Nuclear Magnetic Resonance*; Longman Scientific & Technical: Essex, 1988.

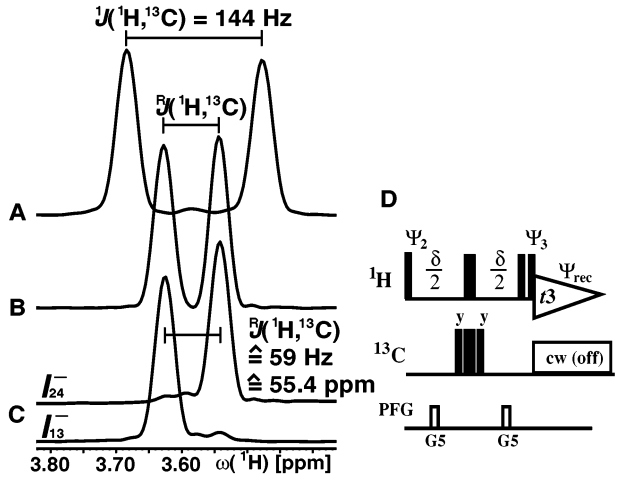

Figure 1. 1D ^{1}H NMR spectra of ^{13}C,^{15}N-labeled leucine showing the ^{1}H$^\alpha$ region: (A) conventional, carbon coupled 1D ^{1}H NMR spectrum, (B) with off-resonance decoupling on ^{13}C, (C) with SITAR on ^{13}C. The component of the doublet selected with the S3E pulse sequence element shown in (D) is marked on the spectrum. In (B) and (C), off-resonance decoupling is applied with a radio frequency power of $\gamma_C B_2/2\pi = 3370$ Hz at a frequency $\omega_{cw} = 64$ ppm. The radio frequency pulses on ^{1}H and ^{13}C are applied at 4.8 and 64 ppm, respectively. The narrow and wide black bars indicate nonselective 90° and 180° pulses, respectively. The line marked PFG indicates a sine shaped magnetic field gradient pulse applied along the *z*-axis (duration 0.5 ms, amplitude 15 G/cm). To suppress passive spin flipping, the delay δ is adjusted to 2.2 ms, which is 0.5 ms longer than $1/(8^1J(^1H,^{13}C))$. The phase cycle is $\Psi_2 = \{45°\}$, $\Psi_3 = \{x\}$, and $\Psi_{rec} = \{x\}$. All other radio frequency pulses are applied either with phase *x* or as indicated above the pulses. A second FID collected with $\Psi_3 = \{-x\}$ is added or subtracted from the first FID, resulting in two subspectra containing one of the two components of the doublet depicted with I^-_{24} and I^-_{13} (the subtracted dataset is phase shifted by 90° from the added dataset). Two scans per experiment are measured using a 10 mM sample of ^{13}C,^{15}N-labeled leucine at 20 °C in D_2O. All experiments reported in this paper are carried out on a Bruker Avance 700 MHz spectrometer equipped with five radio frequency channels and shielded pulsed field gradients along the *z*-direction.

coupling $^1J(I,S)$ and inversely on the chemical shift range of spin *S*, $\omega_{S,max} - \omega_{S,min}$, which has to be covered by the radio frequency field $\gamma_S B_2/2\pi$. Thus, the accuracy of the chemical shift is high for large scalar couplings and a small chemical shift range of spin *S*. Interestingly, the chemical shift resolution (in Hz) in off-resonance decoupling is independent of the external magnetic field *Bo*, because $\omega_{S,max} - \omega_{S,min}$ and the chemical shift resolution along the frequency of spin *I*, which defines the accuracy of the measurement of $^R J(I,S)$, are both proportional to the external magnetic field *Bo*.

Off-resonance decoupling is optimally suited for $t \gg 1/^1J(I,S)$ and thus is preferably applied during acquisition.[14,17,19,21] With off-resonance decoupling during acquisition, the chemical shift of spin *S* is monitored simultaneously with the chemical shift of spin *I*, without the accompanying polarization transfer elements and evolution periods needed in time-domain spectroscopy.[7] The only origin of signal-to-noise loss is in the doublet splitting of the peak due to off-resonance decoupling, which causes a decrease in the signal intensity by a factor of 2. To overcome the potential overlap problems due to the peak splitting, the concept of off-resonance decoupling is combined with spin-state selection.[20] Spin-state selection is achieved by a simple pulse sequence element[20,22−24] (Figures 1D and 2), which selects either I^-_{24} or I^-_{13} resulting in two subspectra with either one of the doublet components. The $^R J(I,S)$ is obtained by measuring the frequency difference between the two individual components in the two subspectra. This E. COSY type of extraction of $^R J(I,S)$ enables an accurate measurement of the residual scalar coupling and concomitantly a precise determination of the chemical shift of spin *S*.

Methods

1D Spin-State Selective Off-Resonance Decoupled (SITAR) ^{1}H Experiment. The concept of SITAR introduced above is applied to the 1D ^{1}H NMR experiment, and the observed spectra are shown in Figure 1C. The single transitions I^-_{24} or I^-_{13} of hydrogens are selected using the S3E element introduced by Meissner et al.[20] Continuous wave off-resonance decoupling is applied during acquisition on ^{13}C (spin *S*). The spin states are selected by the addition or subtraction of two alternate FIDs with pulse sequences that differ by the sign of phase Ψ_3 (see Figure 1D; the subspectrum with I^-_{13} is 90° out of phase). The chemical shift of the carbon attached to the hydrogen is determined by measuring the difference between the doublet components and using eq 6, with the radio frequency power of $\gamma_C B_2/2\pi$ and the actual $^1J(^1H,^{13}C)$. The actual coupling between the spins can be determined using the same experiment with $\gamma_C B_2/2\pi = 0$ Hz.

Pseudo-4D ^{15}N-Resolved [^{15}N−^{1}H,^{1}H−^{15}N]-NOESY Experiment Using SITAR. The concept of SITAR is incorporated into the 3D ^{15}N-resolved [^{1}H,^{1}H]-NOESY experiment for identifying dipolar coupled proton pairs ^{1}H(*i*) and ^{1}H(*j*) by their chemical shifts and the chemical shifts of both of their attached heteronuclei ^{15}N(*i*) and ^{15}N(*j*). The two frequencies of the coupled protons $\omega(^1H(i))$ and $\omega(^1H(j))$ and the heteronuclear frequency $\omega(^{15}N(i))$ are determined using a modified heteronuclear 3D ^{15}N-resolved [^{1}H,^{1}H]-NOESY experiment.[25] The other heteronuclear frequency $\omega(^{15}N(j))$ which is used to characterize the ^{1}H(*j*) spin is obtained by applying SITAR during the acquisition time. The pulse sequence is shown in Figure 2A, and the flow of coherence is explained below in a detailed fashion.

Between time points a and b, magnetization is transferred from ^{1}H(*i*) to ^{15}N(*i*), using a CRINEPT step.[26,27] During the period t_1, ^{15}N(*i*) evolves as multiple quantum coherence. This magnetization (time point *c*) is transferred back to ^{1}H(*i*) via a second CRINEPT step, and the ^{1}H(*i*) spin evolves with $\omega(^1H(i))$ frequency during the evolution period *t*2. The concatenation of evolution time *t*2 and both polarization transfers is implemented in a semiconstant time manner to minimize signal losses due to relaxation and pulse imperfections. In the present approach, up to $\sim^2/_3$ of the evolution time *t*2 is incorporated into the two polarization transfer elements (typical values for a $t2_{max}(^1H(i))$ are ∼15−20 ms and polarization transfer time is ∼10 ms; see Figure 2A). Thus, between time points a and d, the chemical shifts of ^{1}H(*i*) and its attached heteronucleus ^{15}N(*i*) are determined. During the mixing time τ_{mix} (time points d−e), magnetization is transferred via NOE from ^{1}H(*i*) to ^{1}H(*j*). Between time points e and f, the multiplet components I^-_{24} and I^-_{13} are selected using a S3E-element.[20] After the component selection element, the chemical shifts of ^{1}H(*j*) are measured during acquisition *t*3, when off-resonance decoupling is applied on ^{15}N. The difference in the resonance frequencies of the two components from two subspectra yields the residual scalar coupling which has the chemical shift of ^{15}N(*j*). Hence, the chemical shifts of ^{15}N(*j*) are measured indirectly via SITAR (see Theory). The decoupling frequencies and power used are sufficient to scale the residual scalar couplings over the entire range of ^{15}N chemical shift. That is, the residual scalar couplings are almost zero at 102 ppm and almost equal to $^1J(^1H,^{15}N)$ values at 128 ppm.

(22) Sørensen, M. D.; Meissner, A.; Sørensen, O. W. *J. Magn. Reson.* **1999**, *137*, 237−242.
(23) Ottiger, M.; Delaglio, F.; Bax, A. *J. Magn. Reson.* **1998**, *131*, 373−378.
(24) Brutscher, B. *J. Magn. Reson.* **2001**, *151*, 332−338.
(25) Fesik, S. W.; Zuiderweg, E. R. P. *J. Magn. Reson.* **1988**, *78*, 588−593.
(26) Riek, R.; Wider, G.; Pervushin, K.; Wüthrich, K. *Proc. Natl. Acad. Sci. U.S.A.* **1999**, *96*, 4918−4923. Riek, R.; Fiaux, J.; Bertlesen, E. B.; Horwich, A. L.; Wüthrich, K. *J. Am. Chem. Soc.* **2002**, *124*, 12144−12153.
(27) Muller, L. *J. Am. Chem. Soc.* **1979**, *101*, 4481−4484.

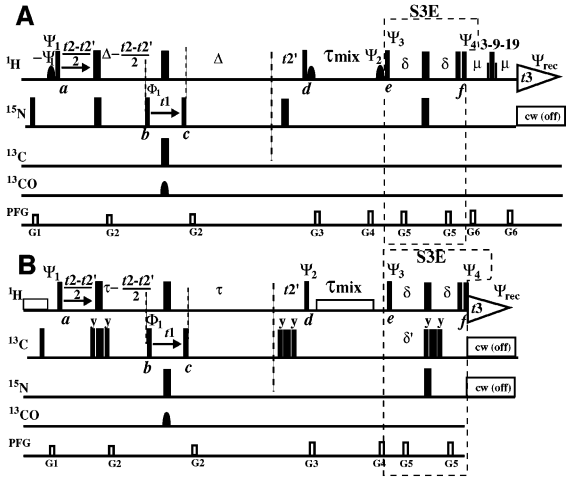

Figure 2. Experimental scheme for (A) the pseudo-4D ^{15}N-resolved [^{15}N−^{1}H,^{1}H−^{15}N]-NOESY experiment and (B) pseudo-4D heavy-atom resolved [^{13}C−^{1}H,^{1}H−^{13}C/^{15}N]-NOESY experiment. (A) The radio frequency pulses on ^{1}H, ^{15}N, ^{13}C are applied at 8.0, 116, and 110 ppm before the mixing time τ_{mix} and switched to 4.7, 102, and 110 ppm during the mixing time, respectively. The narrow and wide black bars indicate nonselective 90° and 180° pulses, respectively. On the line marked ^{1}H, black sine bell shaped pulses indicate selective 90° pulses with the duration of 1 ms and a Gaussian shape truncated at 5%, which are applied on the water resonance. Also, the pulse train 3−9−19 corresponds to an array of pulses 20.77(x)° − λ − 62.21(x)° − λ − 131.53(x)° − λ − 131.53(y)° − λ − 62.21(y)° − 20.77(y)° with λ = 150 μs. The water magnetization stays aligned along the +z-axis throughout the experiment by the use of water flip-back pulses[34] (black sine bell shapes and 3−9−19). The line marked PFG indicates sine shaped magnetic field gradient pulses applied along the z-axis, with the following durations and amplitudes: G1, 1.0 ms, 13 G/cm; G2, 0.1 ms, 7 G/cm; G3, 1.0 ms, 13 G/cm; G4, 1.0 ms, 13 G/cm; G5, 0.5 ms, 9 G/cm; G6, 0.5 ms, 9 G/cm. The delays Δ, δ, and μ are 5.4, 1.5, and 0.6 ms, respectively. τ_{mix}, the NOE mixing time, is 100 ms. The phase cycle is Ψ_1 = {x, x, −x, −x}, Ψ_2 = −Ψ_3, Ψ_3 = {45°, 45°, 45°, 45°, 225°, 225°, 225°, 225°}, Ψ_4 = {x}, Φ_1 = {x, −x}, and Ψ_{rec} = {−x, x, x, −x, x, −x, −x, x}. All other radio frequency pulses are applied either with phase x or as indicated above the pulses. Quadrature detection in the ^{15}N($t1$) or ^{1}H($t2$) dimensions are achieved by the States-TPPI method[33] applied to phase Φ_1 or Ψ_1, respectively. Time-domain spectroscopy of ^{1}H($t2$) is achieved by simultaneous increments (decrements) of the delays $t2'$, 0.5 × ($t2$ − $t2'$), and Δ − 0.5 × ($t2$ − $t2'$). Off-resonance decoupling on ^{15}N is achieved with a continuous field $\gamma_N B_2/2\pi$ = 722 Hz at a frequency ω_{cw} = 102 ppm. The spin-state selection is achieved by recording two free induction decays for each time point, with Ψ_4 = −Ψ_4 and Ψ_2 = −Ψ_2 for the second FID, respectively. The two FIDs are either added or subtracted and phase corrected by 90° in the acquisition dimension. (B) The radio frequency pulses on ^{1}H, ^{15}N, ^{13}C, ^{13}C′ are applied at 8.0, 116, 40, and 175 ppm, respectively. The narrow and wide black bars indicate nonselective 90° and 180° pulses, respectively. The line marked PFG indicates sine shaped magnetic field gradient pulses applied along the z-axis with the following durations and amplitudes: G1, 1.0 ms, 13 G/cm; G2, 0.1 ms, 7 G/cm; G3, 1.0 ms, 13 G/cm; G4, 1.0 ms, 13 G/cm; G5, 0.5 ms, 9 G/cm. The delays δ, δ', and τ are 1.35, 1.55, and 3.5 ms, respectively. τ_{mix}, the NOE mixing time, is 100 ms. The phase cycle used is Ψ_1 = {x, x, −x, −x, y, y, −y, −y}, Ψ_2 = {x, x, x, x, y, y, y, y}, Ψ_3 = {45°, 45°, 225°, 225°}, Ψ_4 = {x}, Φ_1 = {x, x, x, x, −x, −x, −x, −x}, and Ψ_{rec} = {−x, x}. All other radio frequency pulses are applied either with phase x or as indicated above the pulses. Quadrature detection in the ^{13}C($t1$) or ^{1}H($t2$) dimension is achieved by the States-TPPI method[32] applied to phase Φ_1 or Ψ_1, respectively. Time-domain spectroscopy of ^{1}H($t2$) is achieved by simultaneous increments (decrements) of the delays $t2'$, 0.5 × ($t2$ − $t2'$), and τ − 0.5 × ($t2$ − $t2'$). Off-resonance decoupling on ^{15}N is achieved with a continuous field $\gamma_N B_2/2\pi$ = 576 Hz at a frequency ω_{cw} = 102 ppm. Off-resonance decoupling on ^{13}C is achieved with a continuous field $\gamma_C B_2/2\pi$ = 3370 Hz at a frequency ω_{cw} = 70 ppm. The spin-state selection is achieved by recording of two FIDs for each time point with Ψ_4 = −Ψ_4 for the second FID, respectively. The two FIDs are either added or subtracted and phase corrected by 90° in the acquisition dimension. The water magnetization is suppressed by continuous wave during the interscan delay and the mixing time as indicated by white rectangles. Off-resonance decoupling power $\gamma B_2/2\pi$ is calibrated by determining the length of a 180° pulse with the corresponding power.

Spin-state selection is achieved by measuring two FIDs, with pulse sequences differing by the sign of phase Ψ_4. The addition of the two FIDs yields the single transition I^-_{24}, and the subtraction yields I^-_{13}, respectively (see above and Figure 2A). Although using δ = 1/(8^1J(^{1}H,^{15}N)) perfectly selects one of the single transitions, passive spin flipping of ^{15}N(S) introduces partly the other nonselected transition as well, which shows up as an artifact in the spectrum. Passive spin flipping is observed close to the off-resonance decoupling frequency ω_{cw}, because it is stronger with smaller $^R J$(^{1}H,^{15}N) which is true in the vicinity of ω_{cw}. To suppress passive spin flipping, ω_{cw} is set at 102 ppm far from the average ^{15}N chemical shift and δ is set to 1.5 ms (instead of 1.35 ms).[28]

In summary, the coherence flow can thus be described as:

$$^1\mathrm{H}(i)\,[t2] \rightarrow {}^{15}\mathrm{N}(i)\,[t1] \rightarrow {}^1\mathrm{H}(i)\,[t2] \xrightarrow{\text{NOE}} \begin{cases} {}^1\mathrm{H}(j)\exp[\mathbf{i}\{\omega(\mathrm{H}(j)) + \pi\,{}^R J({}^{15}\mathrm{N}(j),{}^1\mathrm{H}(j))\}\,t3] \\ {}^1\mathrm{H}(j)\exp[\mathbf{i}\{\omega(\mathrm{H}(j)) - \pi\,{}^R J({}^{15}\mathrm{N}(j),{}^1\mathrm{H}(j))\}\,t3] \end{cases}$$

where $t1$ and $t2$ are the ^{15}N(i) and ^{1}H(i) evolution times and $t3$ is the ^{1}H(j) acquisition time. The coded ^{15}N((j)) chemical shift is designated in the residual scalar coupling $^R J$(^{15}N(j),^{1}H(j)), which can be extracted from the two subspectra containing either I^-_{24} or I^-_{13} component. The relationship between the ^{15}N(j) chemical shift and $^R J$(^{15}N(j),^{1}H(j)) is given by eq 6.

Pseudo-4D Heavy-Atom Resolved [^{13}C−^{1}H,^{1}H−^{15}N/^{13}C]-NOESY Experiment Using SITAR. The concept of SITAR is also applied to the 3D heavy-atom resolved [^{1}H,^{1}H]-NOESY experiment for identifying dipolar coupled proton pairs ^{1}H(i) and ^{1}H(j) by the chemical shifts of both of their attached heteronuclei ^{13}C(i) and X(j), with X(j) being either ^{15}N or ^{13}C. The two frequencies of the coupled protons ω(^{1}H(i)) and ω(^{1}H(j)) and the heteronuclear carbon frequency ω(^{13}C(i)) are determined using a modified heteronuclear 3D ^{13}C-resolved [^{1}H,^{1}H]-NOESY experiment.[25] The second heteronuclear frequency ω(X(j)), which is used to characterize the ^{1}H(j) spin, is obtained by applying SITAR during the acquisition time. This experiment is similar to the pseudo-4D ^{15}N-resolved [^{15}N−^{1}H,^{1}H−^{15}N]-NOESY discussed in the previous section with the following differences: (i) between time points a and d, ^{1}H magnetization is transferred to ^{13}C accompanied by frequency labeling and transferred back to ^{1}H, (ii) a modified S3E element is used which enables the simultaneous spin-state selection of ^{1}H attached to ^{15}N as well as ^{13}C, and (iii) during acquisition, off-resonance decoupling is applied to both ^{15}N and ^{13}C. Here, the coherence flow is described as follows:

$$^1\mathrm{H}(i)\,[t2] \rightarrow {}^{13}\mathrm{C}(i)\,[t1] \rightarrow {}^1\mathrm{H}(i)\,[t2] \xrightarrow{\text{NOE}} \begin{cases} {}^1\mathrm{H}(j)\exp[\mathbf{i}\{\omega(\mathrm{H}(j)) + \pi\,{}^R J(\mathrm{X}(j),\mathrm{H}(j))\}\,t3] \\ {}^1\mathrm{H}(j)\exp[\mathbf{i}\{\omega(\mathrm{H}(j)) - \pi\,{}^R J(\mathrm{X}(j),\mathrm{H}(j))\}\,t3] \end{cases}$$

where $t1$ and $t2$ are the ^{13}C(i) and ^{1}H(i) evolution times and $t3$ is the ^{1}H(j) acquisition time. The coded X(j) chemical shift is designated in the residual scalar coupling $^R J$(X(j),H(j)). The chemical shift of X(j) can be obtained from $^R J$(X(j),H(j)) using eq 6.

As mentioned above, the important difference between the two NOESY experiments is in the application of the S3E element followed by the off-resonance decoupling. To select one of the transitions of the doublet for both ^{13}C(j) attached ^{1}H(j) and ^{15}N(j) attached ^{1}H(j), the delays δ and δ' should be equal to 1/(8^1J(^{1}H,^{15}N)) and 1/(4^1J(^{1}H,^{15}N)) − 1/(8^1J(^{1}H,^{13}C)), respectively. However, with these values the unselected component of the doublet for the aromatic and aliphatic hydrogens could not be completely suppressed and is observed in the

(28) Meissner, A.; Schulte-Herbruggen, T.; Sørensen, O. W. *J. Am. Chem. Soc.* **1998**, *120*, 7989−7990.

spectrum. These artifacts observed are attributed to the following sources:[28] (i) flipping of the passive spins $^{13}C(j)$ and (ii) J coupling mismatch due to a large variation in $^1J(^1H,^{13}C)$, between approximately 125 Hz to 160 Hz. With the use of $\delta' = 1.55$ ms (see also caption to Figure 2), all of the artifacts due to J coupling mismatch are opposite in sign to that of the selected component. These selection artifacts are expected particularly if the scalar couplings are between 135 and 155 Hz, which is true for aromatic moieties, β moieties of serine and threonine and all of the α moieties. In contrast, passive spin flipping induces artifacts with the sign the same as that of the selected component, and the artifacts close to the decoupling frequency are more intense. Optimizing the value of $\delta' = 1.55$ ms and applying the decoupling frequency close to the α-carbon at 70 ppm, we determined that the artifacts almost cancel due to J coupling mismatch and passive spin flipping (data not shown). The residual artifacts are very weak but opposite in sign to that of the selected component and are therefore easily distinguishable from other (weak) NOEs. As demonstrated by Brutscher,[24] there are alternative spin-state selection filters with significantly reduced sensitivity to J mismatch when compared with the S3E element used here. However, as discussed above, the partial J mismatch produced with the S3E element is desired. Off-resonance decoupling is applied simultaneously on carbon at 70 ppm, with a power $\gamma_C B_2/2\pi$ of 3370 Hz and on nitrogen at 102 ppm with a power $\gamma_N B_2/2\pi$ of 576 Hz. A higher power on ^{13}C would result in a better relation between the residual scalar couplings and ^{13}C chemical shift values. However, the performance of the spectrometer probe head did not allow it. Furthermore, line broadening up to 2 Hz was observed at high decoupling power close to the decoupling frequency due to B_2 inhomogeneity, and line narrowing by ~1 Hz is observed due to partial decoupling of long-range $J(^{13}C,^1H)$ scalar couplings.

Results and Discussion

The Concept of Spin-State Selective Off-Resonance Decoupling (SITAR). To demonstrate the concept of SITAR, it is applied to the 1D ^1H experiment to correlate the chemical shift of ^1H to the chemical shift of the attached ^{13}C. The $^1H^\alpha$ region of a conventional 1D ^1H spectrum of $^{13}C,^{15}N$-labeled leucine is shown in Figure 1A. The $^1H^\alpha$ peak is split by the scalar coupling $^1J(^1H^\alpha,^{13}C^\alpha)$ into two components I^-_{24} or I^-_{13}. When off-resonance decoupling is applied on carbon with a power $\gamma_C B_2/2\pi$ of 3370 Hz at a frequency $\omega_{cw} = 64$ ppm, the residual scalar coupling is scaled in accordance with eq 6 (Figure 1B). SITAR (Figure 1D) selects the doublet components, resulting in two subspectra as shown in Figure 1C, and hence allows an accurate measurement of the residual scalar coupling. Because the residual scalar coupling depends on the chemical shift of ^{13}C (eq 6), the chemical shift of ^{13}C can be obtained and correlated with the chemical shift of ^1H. The accuracy of the ^{13}C chemical shift obtained is <0.1 ppm when compared with conventional time-domain spectroscopy (see also next paragraph). The experimental time required for the SITAR experiment (Figure 1C) is 2 orders of magnitude less than that for a 2D $[^{13}C,^1H]$-correlation experiment with comparable chemical shift resolution along ^{13}C. The SITAR spectrum of Figure 1C is measured in two scans (an additional scan is recorded to get $^1J(^1H^\alpha,^{13}C^\alpha)$, Figure 1A), while a 2D $[^{13}C,^1H]$-correlation experiment with comparable resolution should consist of ~256 complex points along the indirect dimension. Yet the advantage of a 2D experiment is that it is much less prone to resonance overlap. Because of this resonance overlap, off-resonance decoupling is superseded by 2D heteronuclear correlation experiments. However, SITAR is very useful in heteronuclear 3D NMR spectra, where the peaks are well resolved, as discussed in the following section.

Experimental Verification of the Relation Between $^RJ(^1H,X)$ and Chemical Shift of X. From eq 6, it can be seen that SITAR is based on a specific relation between the residual scalar coupling $^RJ(^1H,X)$ and the chemical shift of spin X. To verify the validity of eq 6 and to check the accuracy of the chemical shifts obtained, a 2D combined $[^{13}C,^1H]/[^{15}N,^1H]$-correlation experiment is carried out on a $^{13}C,^{15}N$-labeled ubiquitin sample. The S3E element is added prior to acquisition (see S3E element of the pulse sequence of Figure 2B), and off-resonance decoupling is applied simultaneously on ^{15}N and ^{13}C during acquisition ($\gamma_N B_2/2\pi$ of 390 Hz at a frequency $\omega_{cw} =$ 128 ppm and $\gamma_C B_2/2\pi = 3370$ Hz at a frequency $\omega_{cw} = 70$ ppm, respectively). The resulting two subspectra yield the chemical shifts of ^1H, X, and the corresponding $^RJ(^1H,X)$ per $X-^1H$ moiety (Figure 3A, inset). The residual scalar coupling $^RJ(^1H,^{15}N)$ versus the corresponding ^{15}N chemical shift is shown in Figure 3A, and there is a perfect match between the experimentally observed values and eq 6 (assuming $^1J(^1H,^{15}N)$ to be 92 Hz). Minor deviations are observed between the expected experimental values close to the decoupling frequency ω_{cw} because eq 6 is valid only for ^{15}N resonances far from the decoupling frequency. A careful observation shows that the accuracy and resolution in the chemical shift decreases toward larger residual scalar couplings, because the slope of eq 6 goes toward zero. Nevertheless, the resolution obtained over the entire chemical shift range between 105 and 125 ppm is less than 0.1 ppm (7 Hz at a ^1H frequency of 700 Mz). Prerequisites for this high resolution are the accurate measurement of the residual scalar coupling by E. COSY type techniques and a small (spatial) inhomogeneity of the B_2 field. It should also be noted that the achieved resolution is independent of the static magnetic field (see Theory section).

On the other hand, the correlation between experimental $^RJ(^1H,^{13}C)$ and the corresponding ^{13}C chemical shift is observed to be less accurate than the expected values (Figure 3B). This is due to the $^1J(^1H,^{13}C)$ coupling constant, which is assumed to be 135 Hz in the theoretical curve, although the experimental values vary between 125 and 155 Hz. However, if the corresponding experimentally determined scalar couplings $^1J(^1H,^{13}C)$ are used, the observed chemical shifts are close to the expected values (Figure 3C). Although the scalar couplings measured are very accurate, the ^{13}C chemical shifts are determined only with a standard deviation of 0.4 ppm. Hence, the carbon chemical shifts are less precisely extracted, as compared with the nitrogen chemical shifts (Figure 3A and 3C). This may be due to a partial decoupling of long-range $J(^{13}C,^1H)$ scalar couplings that introduce artifacts to the residual scalar coupling in the order of up to 1 Hz. In addition, the limit on the maximum decoupling power (3370 Hz) which can be applied on the spectrometer probe head yields an unfavorable flat correlation between $^RJ(^1H,^{13}C)$ and the corresponding ^{13}C chemical shifts, in the range between 5 and 30 ppm. Higher decoupling power or a smaller magnetic field at 500 or 600 MHz would increase the slope of the curve and the accuracy of the coded chemical shifts, concomitantly. Furthermore, B_2 inhomogenity introduced by the high decoupling power $\gamma_C B_2/2\pi$ of 3370 Hz covers a large spectral range of approximately 12 000 Hz, resulting in line broadening of up to 2 Hz close to the off-resonance frequency.

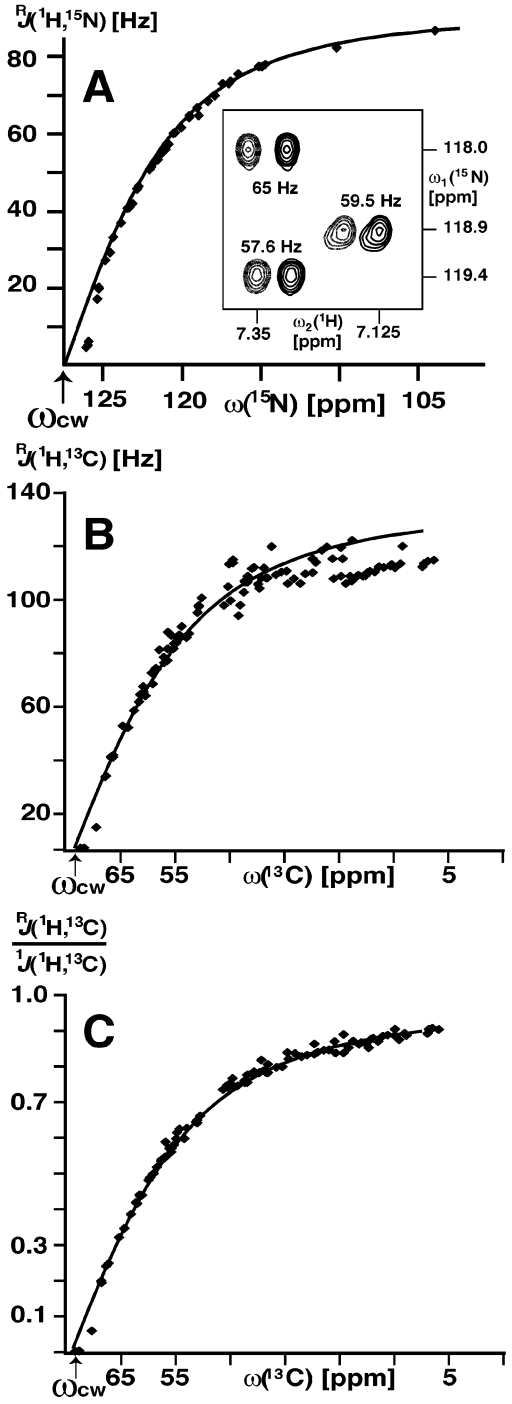

Figure 3. Graph between the chemical shifts and the corresponding residual scalar coupling using SITAR for (A) ^{15}N and (B and C) ^{13}C. Equation 6 is shown as a solid line assuming in (A) the decoupling frequency at ω_{cw} = 128 ppm, of power $\gamma_N B_2/2\pi$ of 576 Hz, and the scalar coupling $^1J(^1H,^{15}N)$ = 92 Hz, and in (B and C) the decoupling frequency at ω_{cw} = 70 ppm, of power $\gamma_C B_2/2\pi$ of 3370 Hz, and the scalar coupling $^1J(^1H,^{13}C)$ = 135 Hz. The experiment is carried out on a sample of ^{13}C,^{15}N-labeled ubiquitin (1 mM concentration, pH 6.5, 20 °C). SITAR is combined with the 2D [^{15}N/^{13}C,^{1}H] correlation experiment, yielding two subspectra with individual multiplet components as shown in the inset. Dashed contour lines correspond to the subspectrum with the component I^-_{13}, and continuous lines correspond to the complementary subspectrum with the component I^-_{24} of the doublet. The measured residual scalar coupling $^RJ(^1H,^{15}N)$ or $^RJ(^1H,^{13}C)$ between the two components is plotted against the corresponding ^{15}N or ^{13}C chemical shifts. In (C), the ratio between the residual scalar coupling $^RJ(^1H,^{13}C)$ and the actual scalar coupling $^1J(^1H,^{13}C)$ is plotted against the ^{13}C chemical shifts. The $^1J(^1H,^{13}C)$ couplings are measured using the same experiment without applying any power for off-resonance decoupling.

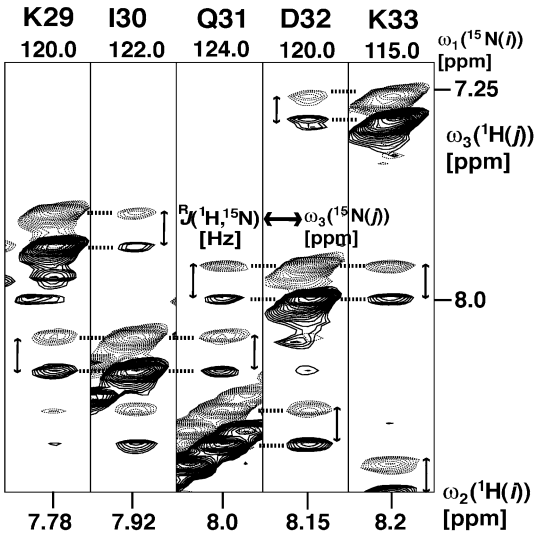

Figure 4. Strips along the $\omega_1(^{15}N)$ dimension of the pseudo-4D ^{15}N-resolved [^{15}N−^{1}H,^{1}H−^{15}N]-NOESY spectrum of a 0.8 mM sample of ^{13}C,^{15}N-labeled ubiquitin, recorded at 20 °C in a mixed solvent of 95% H_2O/5% D_2O at pH 7, using a Bruker Avance 700 MHz spectrometer equipped with five radio frequency channels, a pulsed field gradient unit, and a triple resonance probe with an actively shielded *z*-gradient coil. Dashed contour lines correspond to the subspectrum with the component I^-_{24}, and continuous lines correspond to the complementary subspectrum with the component I^-_{13} of the doublet. The two subspectra are superimposed artificially. The spacing between the two components along $\omega_3(^1H(j))$ corresponds to the residual scalar coupling, which is a function of the ^{15}N chemical shift $\omega_3(^{15}N(j))$ attached to $^1H(j)$. The strips are centered about the corresponding $^1H^N$ chemical shifts. The NOE connectivities are indicated by dashed lines on the basis of the $^RJ(^{15}N,^1H)$ and the chemical shift along $\omega_3(^1H)$. The following parameters are used: data size = 50($t1$) × 85($t2$) × 1024($t3$) complex points; $t1_{max}(^{15}N)$ = 22.5 ms, $t2_{max}(^1H)$ = 20.4 ms, $t3_{max}(^1H)$ = 102 ms. The data set is zero-filled to 128 × 512 × 2048 complex points; 4 × 2 scans per increment are acquired, resulting in 2.5 days of measuring time. Prior to Fourier transformation, the data are multiplied with a 75° shifted sine bell window in all dimensions.

Nevertheless, assuming that $^RJ(^1H,^{13}C)$ scalar couplings are determined with an accuracy of 0.3 Hz, the resolution of the coded chemical shifts through the residual scalar coupling is <0.2 ppm and the chemical shifts can be extracted with a precision of ∼0.4 ppm.

Application of SITAR to Multidimensional NMR Experiments. Pseudo-4D ^{15}N-Resolved [^{15}N−^{1}H,^{1}H−^{15}N]-NOESY. The concept of SITAR is applied to the 3D ^{15}N-resolved [^{15}N−^{1}H,^{1}H−^{15}N]-NOESY experiment for identifying dipolar coupled proton pairs $^1H(i)$ and $^1H(j)$ via the chemical shifts of their attached heteronuclei $^{15}N(i)$ and $^{15}N(j)$. The frequencies of the coupled protons $\omega(^1H(i))$ and $\omega(^1H(j))$ and one of the heteronuclear frequencies $\omega(^{15}N(i))$ are determined as in a standard 3D experiment. The other heteronuclear frequency $\omega(^{15}N(j))$ is obtained by applying SITAR during the acquisition time, and because it gives the same information as that of a 4D experiment, it is referred to as a pseudo-4D NOESY. The experiment is carried out on a ^{13}C,^{15}N-labeled ubiquitin sample, and Figure 4 shows strips from the two subspectra of the pseudo-4D ^{15}N-resolved [^{15}N−^{1}H,^{1}H−^{15}N]-NOESY spectrum. Each peak in the spectrum correlates to four frequencies, $\omega(^1H(i))$ along ω_2, $\omega(^{15}N(i))$ along ω_1, $\omega(^1H(j))$ along ω_3, and $\omega(^{15}N(j))$ indirectly in the splitting between the two components, obtained from two experiments with different phase cycle. The NOE assignment between $^1H(i)$ and $^1H(j)$ is ensured by both doublet components of the cross-peak including the overall position of

the ^{1}H cross-peak as a point of departure (see Figure 4). If the multiplet pattern of the cross-peak on strip *k* coincides with the multiplet pattern of the diagonal peak on strip *l* and vice versa on the other side of the diagonal, the connectivity is traced and ensured by two independent correlations, the ^{15}N chemical shifts and the hydrogen chemical shifts (for example, strip of K29 with the strip of I30 in Figure 4). When the patterns of the doublets do not fit, the two involved ^{15}N−^{1}H moieties are not close in space. It must be noted that the NOEs on both sides of the diagonal do not have the same splitting. Importantly, the proposed procedure for tracing correlations profits from the ^{15}N chemical shifts through the residual scalar coupling and therefore without explicit extraction of the chemical shifts. Therefore, with SITAR the quality of correlation of through-space couplings has improved dramatically, because the correlation can be traced on the basis of ^{15}N and ^{1}H chemical shifts, whereas in the conventional 3D ^{15}N-resolved [^{1}H,^{1}H]-NOESY experiment the correlations are traced only by the ^{1}H chemical shifts. Using the estimated ^{15}N chemical shift accuracy of <0.1 ppm (see above) over the ^{15}N chemical shift dispersion of 30 ppm, we estimated that the additional information of the ^{15}N chemical shift increases the quality of an unambiguous correlation by a factor of ∼300 (see also below).

The corresponding 4D ^{15}N-resolved [^{15}N−^{1}H,^{1}H−^{15}N]-NOESY spectrum also correlates to four frequencies per NOE, $\omega(^1\mathrm{H}(i))$, $\omega(^{15}\mathrm{N}(i))$, $\omega(^1\mathrm{H}(j))$, and $\omega(^{15}\mathrm{N}(j))$, and the assignment is traced on the basis of ^{15}N and ^{1}H chemical shifts. However, the limit on the measuring time, say about 1 week, restricts the complex data points to 85($t1$[^{1}H]) × 16($t2$[^{15}N]) × 16($t3$[^{15}N]) × 1024($t4$[^{1}H acquisition]) that can be measured and hence constraints the resolution dramatically. These data would correspond to a spectral resolution of 25 Hz [^{1}H] × 70 Hz [^{15}N] × 70 Hz [^{15}N] × 4 Hz [^{1}H]. On the other hand, the measured pseudo-4D ^{15}N-resolved [^{15}N−^{1}H,^{1}H−^{15}N]-NOESY spectrum (Figure 4), when measured with the data size of 85($t1$[^{1}H]) × 50($t2$[^{15}N]) × 1024($t3$[^{1}H acquisition]) × 1(spin-state selection) complex points, results in a resolution of 25 Hz [^{1}H] × 22 Hz [^{15}N] × 7 Hz [^{15}N] (indirect) × 4 Hz [^{1}H] and can easily be measured in half of the time. Usually, a 3D experiment (including pseudo-4D experiments) is expected to have more overlap problems in peak assignment than a corresponding 4D experiment. However, the proposed pseudo-4D experiment with two subspectra for the individual multiplet components circumvents this problem, in a simple way. On the other hand, when compared with the conventional 3D version, there is a relaxation-independent signal loss in the intensity by a factor of 2 due to the splitting of the cross-peak, without affecting the volume of the cross-peak. However, this intensity loss is practically independent of the size of the molecule, because the origin of the signal loss is due to the splitting of the cross-peak by the residual scalar coupling and also the duration of the S3E element is short. When the SITAR ^{15}N-resolved [^{15}N−^{1}H,^{1}H−^{15}N] 3D NOESY is compared with the TROSY version, there is a $\sqrt{2}$ relaxation-independent signal gain.[29] Moreover, the implementation profits from concatenation of up to $^2/_3$ of the ^{1}H(i) evolution time $t2$ into the polarization transfer elements, which are transverse relaxation-optimized.[26] Transverse relaxation-optimization[30] is also partially active during the acquisition and $t2$ evolution except during the short $t1$ evolution.

Pseudo-4D Heavy-Atom Resolved [^{13}C−^{1}H,^{1}H−^{15}N/^{13}C]-NOESY Experiment. The concept of SITAR is also applied to the 3D heavy-atom resolved [^{1}H,^{1}H]-NOESY experiment for identifying dipolar coupled proton pairs ^{1}H(i) and ^{1}H(j) via the chemical shifts of their attached heteronuclei ^{13}C(i) and ^{15}N(j) or ^{13}C(j) (the experiment is set up to cover also the aromatic carbons for both ^{13}C(i) and ^{13}C(j)). The frequencies of the coupled protons $\omega(^1\mathrm{H}(i))$ and $\omega(^1\mathrm{H}(j))$ and the heteronuclear frequencies of the attached carbon or nitrogen $\omega(^{13}\mathrm{C}(i))$ and $\omega(^{15}\mathrm{N}(j)$ or $^{13}\mathrm{C}(j))$ are obtained from this experiment. The heteronuclear frequency $\omega(^{15}\mathrm{N}(j)$ or $^{13}\mathrm{C}(j))$ is obtained by applying SITAR during the acquisition time. Hence, this experiment is similar to the pseudo-4D ^{15}N-resolved [^{15}N−^{1}H,^{1}H−^{15}N]-NOESY experiment discussed in the previous section, and therefore only the advantages and the limitations of this experiment will be discussed here. Figure 5 shows planes from the two subspectra of the pseudo-4D heavy-atom resolved [^{13}C−^{1}H,^{1}H−^{15}N/^{13}C]-NOESY spectrum of ^{13}C,^{15}N-labeled ubiquitin. Each peak in the spectrum correlates to four frequencies, $\omega(^1\mathrm{H}(i))$ along ω_2, $\omega(^{13}\mathrm{C}(i))$ along ω_1, $\omega(^1\mathrm{H}(j))$ along ω_3, and indirectly $\omega(^{15}\mathrm{N}(j)$ or $^{13}\mathrm{C}(j))$ in the frequency difference between the two components of the doublet, obtained by two experiments carried out with a different phase cycle. Importantly, the proposed procedure for tracing correlations profits from the ^{13}C chemical shifts through the residual scalar coupling, without explicit extraction of the chemical shifts.

The assignment of correlations by the proposed pattern recognition uses the ^{13}C chemical shift encoded in the residual scalar coupling with a resolution of ∼0.2 ppm, although the correlation between ^{13}C chemical shift and residual scalar coupling is not well defined without the knowledge of the $^1J(^1\mathrm{H},^{13}\mathrm{C})$ scalar couplings (Figure 3B). Using the estimated ^{13}C/^{15}N chemical shift resolution of less than 0.2 or 0.1 ppm, and a ^{13}C/^{15}N chemical shift dispersion of 60 or 30 ppm, we estimated that the additional information of the ^{15}N/^{13}C chemical shift increases the quality of an unambiguous correlation by a factor of ∼300 (see also below). The corresponding 4D ^{13}C-resolved [^{13}C−^{1}H,^{1}H−^{13}C]-NOESY experiment also contains all four frequencies per NOE. However, the limit on the measuring time of say about 1 week constraints the spectral resolution dramatically. For example, with the complex data size of 85($t1$[^{1}H]) × 16($t2$[^{13}C]) × 16($t3$[^{13}C]) × 1024($t4$[^{1}H acquisition]), the achievable spectral resolution is 25 Hz [^{1}H] × 170 Hz [^{13}C] × 170 Hz [^{13}C] × 4 Hz [^{1}H] (taking into account the possible folding of the ^{13}C dimension). On the other hand, with the same data size from the pseudo-4D [^{13}C−^{1}H,^{1}H−^{13}C/^{15}N]-NOESY spectrum (Figure 5), a resolution of 25 Hz [^{1}H] × 60 Hz [^{13}C] × 7 Hz [^{15}N] or 34 Hz [^{13}C] (indirect) × 4 Hz [^{1}H] is possible. Furthermore, the proposed pseudo-4D [^{13}C−^{1}H,^{1}H−^{13}C/^{15}N]-NOESY contains the aromatic NOEs (with a residual scalar coupling > 100 Hz at ^{1}H chemical shifts > 6 ppm), and also [^{13}C−^{1}H,^{1}H−^{15}N]-NOEs (with a residual scalar coupling < 92 Hz at ^{1}H chemical shifts > 6 ppm), in addition to the aliphatic NOEs (with a residual scalar coupling

(29) Zhu, G.; Kong, X. M.; Sze, K. H. *J. Biomol. NMR* **1999**, *13*, 77−81.

(30) Pervushin, K.; Riek, R.; Wider, G.; Wüthrich, K. *Proc. Natl. Acad. Sci. U.S.A.* **1997**, *94*, 12366−12371. Riek, R.; Pervushin, K.; Wüthrich, K. *Trends Biochem. Sci.* **2000**, *25*, 462−468. Riek, R. *Methods and Principles in Medicinal Chemistry*; Wiley-VCH: Weinheim, Germany, 2003; Vol. 16, pp 227−241.

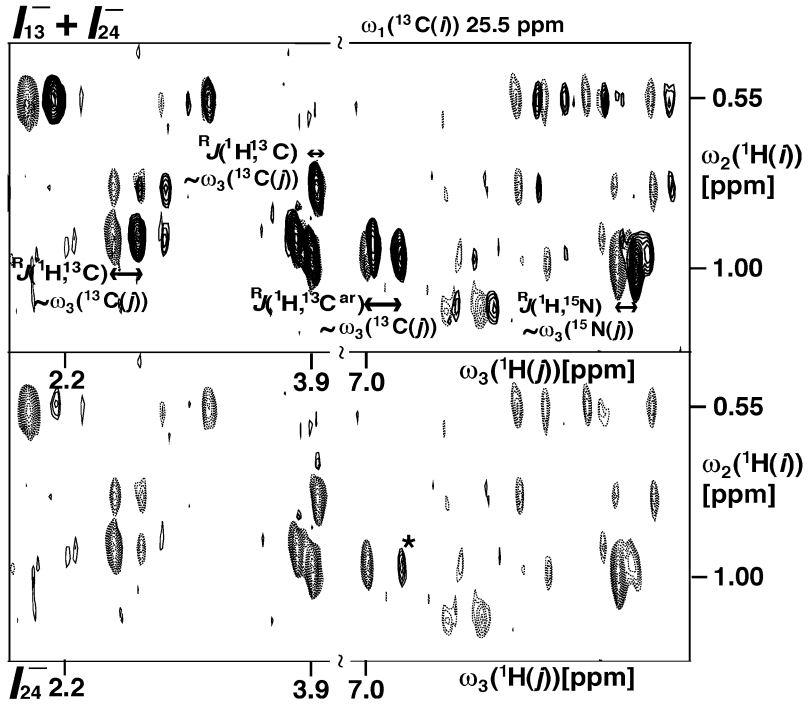

Figure 5. $\omega_1(^{13}C)$-plane of the pseudo-4D heavy-atom resolved [$^{13}C-^1H,^1H-^{15}N/^{13}C$]-NOESY spectrum of $^{13}C,^{15}N$-labeled ubiquitin. Dashed contour lines correspond to the subspectrum with the component I^-_{24}, and continuous lines correspond to the complementary subspectrum with the component I^-_{13} of the doublet. The two subspectra are superimposed artificially. The spectrum shown below corresponds to only the subspectrum with the component I^-_{24}. The spacing between the two components along $\omega_3(^1H(j))$ corresponds to the residual scalar coupling, which is a function of the chemical shift $\omega_3(^{13}C(j)$ or $^{15}N(j))$ of the attached heavy atom as indicated on the spectrum. Designated with "*" is an artifact peak due to *J* mismatch. The experiment is recorded at 700 MHz ^1H frequency, at 20 °C with a 0.8 mM sample of $^{13}C,^{15}N$-labeled ubiquitin in a mixed solvent of 95% H_2O/5% D_2O at pH 7. The following parameters are used: data size = 50(*t*1) × 150(*t*2) × 512(*t*3) complex points; $t1_{max}(^{13}C) = 7$ ms, $t2_{max}(^1H) = 15$ ms, $t3_{max}(^1H) = 51$ ms. The data set is zero-filled to 128 × 512 × 2048 complex points; 4 × 2 scans per increment are acquired, resulting in 2.5 days of measuring time. Prior to Fourier transformation, the data are multiplied with a 75° shifted sine bell window in all dimensions.

between 0 and 155 Hz at ^1H chemical shifts < 6 ppm). Thus, with the pulse sequence of Figure 2B, all of the NOEs can be observed and are easily distinguished.

The imperfect selection of one of the doublet components, which results from passive spin flipping and *J* mismatch due to the large variation of $^1J(^1H,^{13}C)$ scalar couplings, yields weak residual artifacts. These artifacts can be easily distinguished from NOEs as they are always opposite in sign to that of the selected component. It should be also mentioned that the application of SITAR in the pseudo-4D ^{13}C-resolved [$^{13}C-^1H,^1H-^{13}C/^{15}N$]-NOESY experiment is highly demanding, because the chemical shift range of the carbon to be covered by off-resonance decoupling is large and the scalar couplings are inhomogeneous. Nonetheless, the proposed pseudo-4D ^{13}C-resolved [$^{13}C-^1H,^1H-^{13}C/^{15}N$]-NOESY experiment supersedes the conventional NOESY experiment by 2 orders of magnitude in spectral resolution.

Unambiguous Identification of NOEs by SITAR-Based Resolution Enhancement. The strength of SITAR applied to the NOESY experiment lies in the increase of the spectral resolution by 2 orders of magnitude. Therefore, it helps in unambiguously identifying dipolar coupled proton pairs by the chemical shifts of both of their attached heteronuclei. Figure 6 shows several examples of ambiguities, which can be resolved by SITAR-based detection of the chemical shift of the corresponding heteronucleus attached to the protons. Using only the dashed subspectrum of Figure 6A, which serves as a representative of a 3D ^{13}C-resolved [$^1H,^1H$]-NOESY spectrum, we could not unambiguously assign the NOEs, because of the degeneracy in the chemical shift of ^{1}HN Ile 61 and $^1H\epsilon$ Phe 4 along $\omega_3(^1H)$. However, with the use of both subspectra, the NOE can be unambiguously assigned to either ^{1}HN Ile 61 and $^1H\epsilon$ Phe 4 due to the ^{15}N or ^{13}C chemical shifts measured in the SITAR dimension $\omega_3(^{15}N/^{13}C)$. Similarly, in the dashed subspectrum of Figure 6B, which serves as a representative of a 3D ^{13}C-resolved [$^1H,^1H$]-NOESY spectrum, ^{1}HN of Arg 42 cannot be distinguished from ^{1}HN Glu 51, because both of them have identical chemical shifts along $\omega_3(^1H)$. Therefore, a large number of NOEs, nine of which are displayed in Figure 6B, cannot be assigned or grouped into the two classes shown, unless the corresponding ^{15}N chemical shift coded in the splitting between the two subspectra is taken into account. The final example of Figures 6C shows that only the use of the residual scalar coupling, which codes the ^{13}C chemical shift along the SITAR dimension $\omega_3(^{13}C)$, enables an unambiguous assignment of the cross-peaks to either $^1H\alpha$ Gly 10 or $^1H\alpha$ Lys 11. These examples are only three out of many, because every ^1H chemical shift degeneracy results in a set of ambiguous NOEs. Indeed, a statistical analysis shows that only 15% of the NOEs in a 3D ^{13}C-resolved [$^1H,^1H$]-NOESY spectrum of $^{13}C,^{15}N$-labeled ubiquitin can be unambiguously assigned with a chemical shift resolution along ^1H of 0.02 ppm and along ^{13}C dimension of 0.4 ppm, respectively. This observation is consistent with an experimental and theoretical analysis of Mumenthaler and coworkers.[32] They demonstrated with a simple mathematical model, which is described in the caption to Figure 7, that for a

(31) Melacini, G. *J. Am. Chem. Soc.* **2000**, *122*, 9735−9738.

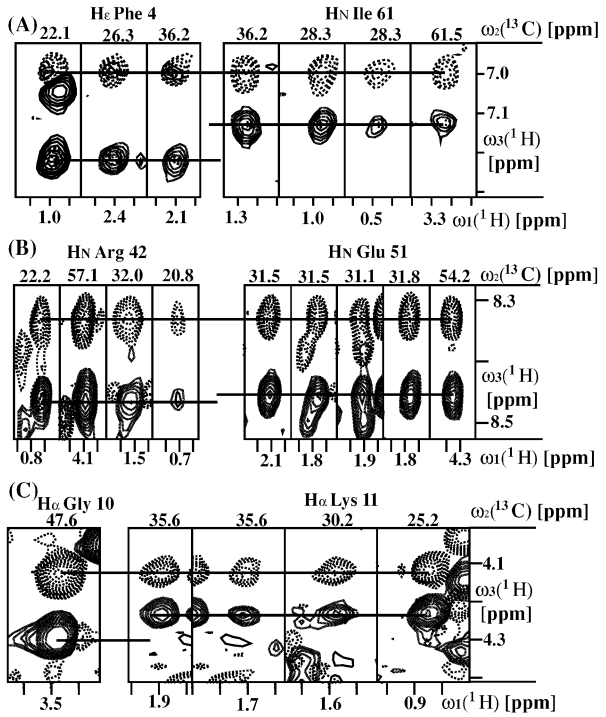

Figure 6. Examples of NOEs which can be unambiguously assigned using the SITAR-based pseudo-4D heavy-atom resolved [^{13}C−^{1}H,^{1}H−^{15}N/^{13}C]-NOESY experiment. Dashed contour lines correspond to the subspectrum with the component I^{-}_{24}, and continuous lines correspond to the complementary subspectrum with the component I^{-}_{13} of the doublet. The two subspectra are superimposed artificially. The chemical shifts of the individual slices are given on the top for $\omega_2(^{13}C)$, on the right of the spectrum for $\omega_3(^{1}H)$, and on the bottom for $\omega_3(^{1}H)$, respectively. The spacing between the two components along $\omega_3(^{1}H(j))$ corresponds to the residual scalar coupling, which is a function of the ^{15}N or ^{13}C chemical shift $\omega_3(^{15}N(j))$ or $\omega_3(^{13}C(j))$ attached to $^{1}H(j)$. The given assignments are indicated by lines along $\omega_3(^{1}H)$ and can only be assigned using the SITAR dimension. For example, the multiplet component I^{-}_{24} of cross-peaks of ^{1}HN Ile 61 or $^{1}H\epsilon$ Phe4 have exactly the same chemical shift in the dashed subspectrum along $\omega_3(^{1}H)$ as indicated by one straight line, and therefore the assignment is ambiguous. Because the component I^{-}_{13} values of the two amide protons are different, the NOEs shown can be grouped and assigned unambiguously to ^{1}HN Ile 61 or $^{1}H\epsilon$ Phe 4 as labeled. The spectral parameters are given in Figure 5.

typical protein data set less than 10% of the NOEs can be assigned unambiguously.[32] Furthermore, this model predicts that the number of unambiguous NOEs decreases exponentially with the increase in the size of the protein (Figure 7). Nonetheless, with a complete chemical shift list (>90%), reliable automated NOESY assignment and structure determination procedures have been developed using a series of tricks, that is, symmetry-related cross-peaks, network anchoring, and cycles of intermediate structure determination and assignment.[3,4] For example, the use of symmetry-related cross-peaks in Figure 6C enables NOE assignment in a conventional 3D NOESY spectrum (symmetry-related cross-peaks not shown). However, the ambiguities of the NOEs of Figure 6A and 6B cannot be lifted from symmetry-related cross-peaks, because they do not exist due to the nature of the experiment.

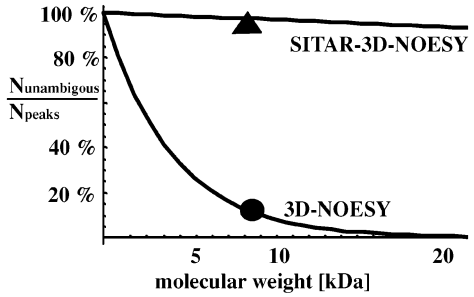

Figure 7. Theoretical calculation of the percentage of unambiguous NOEs ($N_{unambiguous}$) versus total number of NOEs (N_{peaks}) as a function of the molecular weight of the protein studied using conventional 3D-resolved [^{1}H,^{1}H]-NOESY spectra and SITAR-based pseudo-4D heavy-atom resolved [^{1}H,^{1}H]-NOESY spectra. The curves are calculated using a simple mathematical model introduced by Mumenthaler and co-workers:[32] N is the total number of nondegenerate hydrogen atoms, N_{peaks} is the total number of peaks in the spectrum, $\Delta(^{1}H)$ is the spectral resolution, and $\Delta\omega(^{1}H)$ is the chemical shift range within the vast majority of the proton chemical shifts are located. Assuming that the proton shifts are distributed evenly over the region $\Delta\omega(^{1}H)$ results in the probability $p = 2\Delta(^{1}H)/\Delta\omega(^{1}H)$ of finding a proton shift in an interval $2 \times \Delta(^{1}H)$. Furthermore, it is assumed that there is no ambiguity in the proton dimension correlated directly to the heterospin ($\omega_1(^{1}H)$ dimension with $\omega_2(^{15}N/^{13}C)$ dimension).[32] The percentage of peaks with only one possible unambiguous assignment is then given by $N_{unambiguous}/N_{peaks} = (1 - p)^{N-1} \approx \exp[-Np]$. In the SITAR spectra, the probability is given by $p = 2\Delta(^{1}H)/\Delta\omega(^{1}H) \times 2\Delta(^{15}N/^{13}C)/\Delta\omega(^{15}N/^{13}C)$ where $\Delta(^{15}N/^{13}C)$ is the spectral resolution along the pseudo-dimension and $\Delta\omega(^{15}N/^{13}C)$ is the chemical shift range of the corresponding heavy atoms. The following values have been used for the calculation: $\Delta\omega(^{1}H) = 9$ ppm, $\Delta(^{1}H) = 0.02$ ppm,[32] $\Delta\omega(^{15}N/^{13}C) = 30$ ppm/60 ppm, $\Delta(^{15}N/^{13}C) = 0.2$ ppm/0.4 ppm, respectively. The number of nondegenerate hydrogen atoms per 1 kDa is set to 40. This number is based on a small statistics of proteins studied by NMR in our laboratory and on the paper of Mumenthaler et al.[32] In addition, $N_{unambiguous}/N_{peaks}$ values of the ^{13}C-resolved [^{1}H,^{1}H]-NOESY spectrum (●) and pseudo-4D heavy-atom resolved [^{13}C−^{1}H,^{1}H−^{15}N/^{13}C]-NOESY spectrum (▲) of ^{13}C,^{15}N-labeled ubiquitin are given. The number of unambiguous NOEs $N_{unambiguous}$ were determined using a $\Delta(^{1}H)$ of 0.02 ppm and $\Delta(^{13}C)$ of 0.4 ppm, respectively.

As can be inferred from Figure 7, the number of unambiguous NOEs using SITAR technology is predicted to be ∼90−100%. Indeed, >90% of the NOEs observed in the 4D heavy-atom resolved [^{13}C−^{1}H,^{1}H−^{15}N/^{13}C]-NOESY spectrum of ^{13}C,^{15}N-labeled ubiquitin are unambiguous (Figure 7). Thus, SITAR-based NOESY spectra change dramatically the requirement of automated NOESY assignment and structure determination: (i) the automated NOESY assignment and structure determination with an incomplete sequential assignment should be straightforward. (ii) Automated structure determination should be possible with backbone assignment only. The side chain assignment would be achieved automatically and in parallel to the automated NOESY assignment and structure determination during the calculation. (iii) De novo structure determination without any sequential assignment should be possible using the "CLOUD" approach, recently successfully implemented by Grishaev and Llinas.[5] The "CLOUD" approach determines the structure on the basis of the collection of unambiguous NOEs which are translated into a proton density map using relaxation matrix analysis. The proton density map is then used to generate the three-dimensional structure of the protein. The major bottleneck of this approach is the need for a large collection of unambiguous NOEs between two unassigned but unambiguous protons. It is therefore evident that the combination of the SITAR technique with the "CLOUD" approach might enable fully automated structure determination of proteins.

(32) Mumenthaler, C.; Guntert, P.; Braun, W.; Wüthrich, K. *J. Biomol. NMR* **1997**, *10*, 351−362. Guntert, P. *Methods and Principles in Medicinal Chemistry*; Wiley-VCH: Weinheim, Germany, 2003; Vol. 16, pp 39−66.
(33) Marion, D.; Ikura, M.; Tschudin, R.; Bax, A. *J. Magn. Reson.* **1989**, *85*, 393−399.
(34) Grzesiek, S.; Bax, A. *J. Am. Chem. Soc.* **1993**, *115*, 12593−12594.
(35) Herrmann, T.; Guntert, P.; Wuthrich, K. *J. Mol. Biol.* **2002**, *319*, 209−227.

Conclusions

SITAR is a new technique for the detection of chemical shift information in multidimensional experiments. The strength of spin-state selective off-resonance decoupling (SITAR) lies in the increase of the spectral resolution by 2 orders of magnitude without major signal losses. Therefore, the implementation of SITAR to the NOESY experiment helps in unambiguously identifying dipolar coupled proton pairs by the chemical shifts of both of their attached heteronuclei. The increase in unambiguous identification of NOEs by SITAR-based resolution enhancement is very important, because less than 10% of the NOEs can be assigned unambiguously for a typical protein data set.[32] The SITAR technique can also be used to distinguish intermolecular and intramolecular NOEs in $^{13}C,^{15}N$-labeled protein and unlabeled ligand interactions, where there is no splitting in the intermolecular NOEs.[31] Hence, it is intriguing to speculate that the large collection of unambiguous dipolar coupled proton pairs provided by SITAR-based NOESY experiments opens an avenue for the 3D structure determination of $^{13}C,^{15}N$-labeled proteins and protein complexes without sequential assignments using the "CLOUD" approach.[5] This would result in a fully automated protocol for structure determination of proteins.

Although the SITAR technique has been shown to be useful for identifying dipolar coupled spin pairs, the concept can be extended to scaling large dipolar couplings in oriented biomolecules. Furthermore, the straightforward implementation of SITAR opens the technique to a large variety of applications including high-throughput efforts for backbone resonance assignment. Indeed, preliminary results with SITAR applied to triple resonance experiments are promising, because the dimensionality can be decreased without resolution losses and concomitantly triple resonance experiments can be measured in a very short time.

Acknowledgment. The financial support of the H. and J. Weinberg Foundation, the H. N. and F. C. Berger Foundation, and the Auen Foundation has been gratefully acknowledged.

JA035689X